Journal of Inorganic Biochemistry 280 (2026) 113309

Contents lists available at ScienceDirect

Journal of Inorganic Biochemistry

journal homepage: www.elsevier.com/locate/jinorgbio

Structural and functional role of the magnesium ion in the human oxytocin receptor

Francesco Musiani [a,1,*], Samira Al Sadi [a,b,1], Alejandro Giorgetti [c], Mercedes Alfonso-Prieto [d], Paolo Carloni [d,e,f,g,**]

[a] Laboratory of Bioinorganic Chemistry, Department of Farmacy and Biotechnology, University of Bologna, Bologna, Italy
[b] Present address: Department of Inorganic and Organic Chemistry & IQTCUB, University of Barcelona, Barcelona, Spain
[c] Department of Biotechnology, University of Verona, Verona, Italy
[d] Institute of Neuroscience and Medicine (INM-9), Computational Biomedicine, Forschungszentrum Jülich, Jülich, Germany
[e] JARA-HPC, Forschungszentrum Jülich, Jülich, Germany
[f] Department of Physics, RWTH Aachen University, Aachen, Germany
[g] JARA Institute Molecular Neuroscience and Neuroimaging (INM-11), Forschungszentrum Jülich, Jülich, Germany

ARTICLE INFO

Keywords:
Oxytocin
Oxytocin receptor
Mg^{2+} mediated binding
Molecular dynamics

ABSTRACT

The binding of the oxytocin cyclic peptide to its target oxytocin receptor plays a key role for human behaviour. Both binding and receptor activation are affected by the presence of a Mg^{2+} ion. Unfortunately, the current experimental structural information does not provide a complete picture of the metal coordination chemistry. Here, by using molecular dynamics and taking advantage of an ad hoc force field for the divalent ion, we predict the location of four water molecules completing the octahedral coordination of the metal ion. We also suggest that binding of oxytocin is enhanced by the simultaneous proximity of the C-terminal region of oxytocin and the N-terminal region of the receptor to the Mg^{2+} ion, while activation also depends on the conformation of transmembrane helices 5 and 6 joined by intracellular loop 3, a region that has not been solved in experimental structures and that has been modelled here in two conformations using state-of-the-art techniques.

1. Introduction

With about 800 known members, G protein-coupled receptors (GPCRs) are the largest transmembrane receptor superfamily in the human genome [1]. They are of crucial pharmaceutical importance, being targeted by about one third of marketed drugs [2]. In recent years, the modulatory role of metal ions in GPCRs' function has been increasingly recognized [3,4]. Two main ion binding modes have been observed [4]. The most well characterized is that of Na^{+} in the allosteric site containing $D^{2.50}$ (using the Ballesteros-Weinstein generic GPCR numbering scheme), highly conserved in *class A* GPCRs, which was found to stabilize the inactive receptor conformation [3]. Nonetheless, this allosteric ion binding site can also be occupied by Ca^{2+} in a subset of *class A* GPCRs that contain a second acidic residue near $D^{2.50}$, including olfactory receptors [5]. In addition, metal ions can also bind in the same orthosteric site where the endogenous ligand binds to the GPCR. For instance, Ca^{2+} and Zn^{2+} act as positive allosteric modulators of melanocortin receptors by interacting simultaneously with the agonist and the receptor [6–12]. Similarly, Mg^{2+} enhances agonist affinity and receptor signalling in the μ-opioid receptor [13,14] by bridging the ligand and the receptor.

Magnesium ions are integral to numerous biological processes across a wide range of living organisms. As one of the most abundant elements in the human body, Mg^{2+} ions act as cofactors in over 300 enzymatic systems that govern a wide range of biochemical processes in the body, such as protein synthesis, muscle and nerve function, blood sugar regulation, and blood pressure control [15–18]. On the other hand, Mg^{2+} ions deficiency appears to be involved in various mental health disorders, including anxiety and depression [16,19–21] as well as in dementia development [22]. A paradigmatic example of the role of Mg^{2+} ions in GPCRs is represented by oxytocin (OT, Fig. 1A), a signalling cyclic peptide consisting of nine residues that functions as both a

* Corresponding author at: F. Musiani, Via Piero Gobetti 87, 40129 Bologna, Italy.
** Corresponding author at: P. Carloni, Wilhelm-Johnen-Straße, 52428 Jülich, Germany.
E-mail addresses: francesco.musiani@unibo.it (F. Musiani), p.carloni@fz-juelich.de (P. Carloni).
[1] FM and SAS contributed equally to this work.

https://doi.org/10.1016/j.jinorgbio.2026.113309
Received 5 November 2025; Received in revised form 11 February 2026; Accepted 10 March 2026
Available online 10 March 2026

hormone and a neurotransmitter [23–26]. Its cyclic structure is stabilized by a disulfide bond between its two cysteines. OT is ubiquitous across the animal kingdom, where it exerts diverse central and peripheral effects. In mammals, its main physiological target is a *class A* GPCR, the oxytocin receptor (OTR) [23,27,28], where it acts as an agonist. The peripheral activation of the OTR is closely linked to parturition and lactation. As neurotransmitter, it regulates the development and maintenance of complex mammalian behaviours, from sexual arousal to mother-cub bonding [29]. Selective activation of the OTR in humans may help mental health conditions, including autism spectrum disorders, social anxiety disorder, and schizophrenia [30,31]. In addition, naturally occurring genetic variants of the OTR have been associated to several disorders [32,33]. The binding of OT to OTR is enhanced by the presence of a Mg^{2+} ion (or a related cation) [34–36]. The OTR active state cryo-EM structures in complex with OT and a G_q protein, either in the absence (PDB ID 7QVM, 0.325 nm resolution [37]) or in the presence of a Mg^{2+} ion (Fig. 1B, PDB ID 7RYC, 0.290 nm resolution [28]) have provided crucial information on the functional role of the metal ion.[2] The GPCR seven-transmembrane helices (TM1-TM7) bundle is connected by intracellular loops (ICL1–3, that are 6, 5, and 37 residues long, respectively) and extracellular loops (ECL1–3, that are 5, 20, and 8 residues long, respectively). The long ICL3 is a modulatory domain: its conformational flexibility determines the accessibility of the receptor's G protein interaction site [38,39]. ECL2 assumes an elongated β-hairpin configuration attached to the extracellular terminus of TM3 via a disulfide bridge, as observed in other *class A* peptide-binding GPCRs [28,37,40]. The C-terminal amphipathic eighth helix positioned parallel to the membrane is involved in the binding of its cognate G-protein (Fig. 1B). In both structures, OT adopts a nearly planar orientation within the binding pocket (Fig. 1B) and is positioned almost perpendicular to the membrane plane. The cyclic region of OT binds deep in the orthosteric binding site, while the C-terminal tripeptide extends toward the extracellular loops and binds to the OTR N-terminal region plus ECL2 and ECL3 (Fig. 1B and Fig. S1 in the Supplementary Material).

In the metal bound form, the Mg^{2+} ion interacts directly with D100 (Fig. 1C) in the extracellular tip of TM2, while a second acidic residue (E42), in the extracellular tip of TM1, is also in its proximity (Mg^{2+}-E42 (Oε1) distance = 0.40 nm), suggesting (but not proving) a water-mediated interaction, as metal-bound water molecules have not been observed in the cryo-EM structures. This under-coordination of the metal ion is at odds with the octahedral coordination observed for Mg^{2+}-bound structures in the Protein Data Bank [41–43]. The extracellular loop regions and the N-terminal domain stabilize the OT binding site by forming a ligand-capping complex (Fig. S1). In particular, Pro^7 interacts with I312, M315 and the Mg^{2+} second coordination shell, including R34 in the N-terminal domain.

This structural information provides the molecular basis of the experimentally observed decrease of OT affinity upon loss of the metal ion [44]. However, the coordination sphere of Mg^{2+} has not been fully characterized, though it was proposed that the presence of ligand water molecules could explain the Mg^{2+} selectivity over Ca^{2+} [28]. Moreover, the available cryo-EM structures also suggest that the peptide affinity drop is slightly reduced by using the [Thr^4,Gly^7]OT [44] OT analogue [45,46], as OT loses the stabilizing interactions of the residues in position 7. However, this structural information does not explain why OT binding without the metal ion is reduced even more [44] by inverting the Tyr^2 Cα configuration ([D-Tyr^2]OT analogue [47]), nor why the

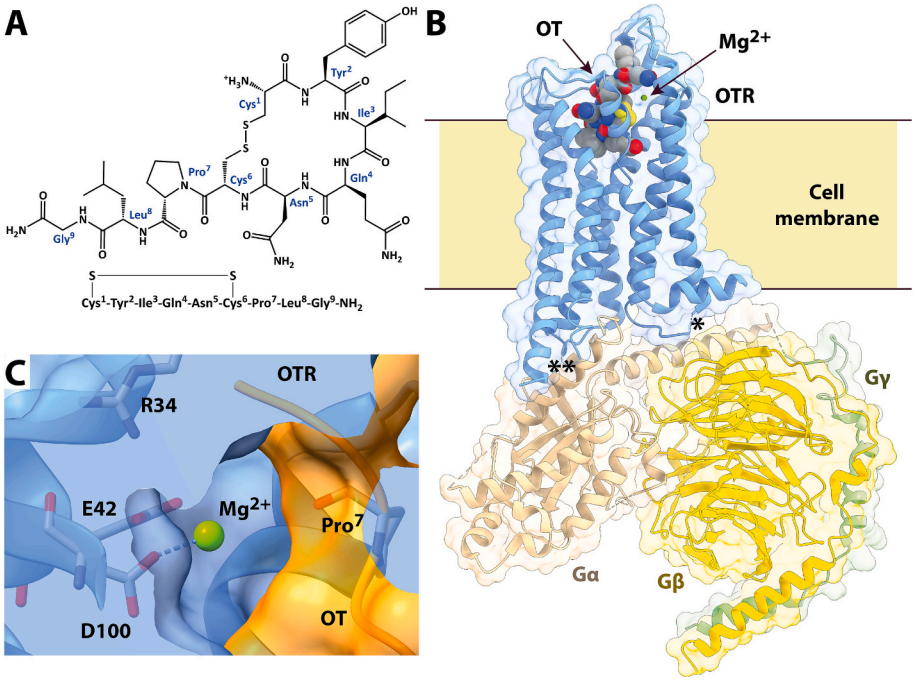

Fig. 1. (**A**) Scheme and sequence of the OT nonapeptide highlighting the presence of a disulfide bridge between Cys^1 and Cys^6 and of the amidated C-terminal. (**B**) Ribbon scheme of the OTR cryo-EM structure in complex with a heterotrimeric G_q protein and bound to OT and a single Mg^{2+} ion used in this study (PDB ID 7RYC) [28]. OTR is in light blue ribbons while the G_q protein subunits are in tan (Gα), yellow (Gβ) and light green (Gγ). OT and the Mg^{2+} ion are reported as spheres coloured according to the atom type. The OTR unmodelled regions are indicated by a * for ICL2 and by ** for the 30 residues stretch in the TM5-ICL3-TM6 region. The position of the cell membrane is also indicated. (**C**) Detail of the Mg^{2+} binding site as found in the experimental structure, showing an under-coordinated metal ion. The ribbons and the molecular surfaces of OTR and OT are in light blue and orange, respectively. The Mg^{2+} ion is reported using a green sphere, while selected residues cited in the text are in sticks coloured according to the atom type. (For interpretation of the references to colour in this figure legend, the reader is referred to the web version of this article.)

[2] From hereafter, the amino acids three letter code with superscript numeration has been used for OT residues (e.g., Pro^7), while the single letter code refers to receptor residues (e.g., D100).

presence of magnesium enhances not only OT binding but also OTR activation.

Here, we performed atomistic molecular dynamics (MD) simulations on the Mg^{2+}-bound OTR in complex with OT in an effort to address these two important issues. Because the experimental structure lacked two main regions (Fig. 1B): *i*) residue 68 in ICL2 and *ii*) a 30-residue stretch (residues 237–265) constituting the TM5-ICL3-TM6 region, we added them using the receptor cryo-EM structure as a template, aided by AlphaFold-Multistate [48] (see Supplementary Material for full Methods details). The latter produced two different conformations for the TM5-ICL3-TM6 region: one featuring TM6 broken into two sub-helices (hereafter OTRb) and a second showing an elongated helix (OTRe) (Fig. 2A). For each of the two conformations, three 1 μs-long replica simulations were performed. In all the simulations OTR was embedded in a lipid bilayer composed of 70% 1-palmitoyl-2-oleoyl-sn-glycero-3-phosphocholine (POPC) and 30% cholesterol (CHL) and solvated in a solution at physiological ionic strength (Fig. S2). The cholesterol percentage was chosen based on the average composition found in the two leaflets of the typical mammalian plasma membrane [49]. The effect of membrane lipid composition on OTR has been recently remarked by extensive atomistic MD simulations focusing on CHL interaction sites [50], as well as previous experimental data [51].

2. Results and discussion

Here we present results from our three-replica, microsecond-long MD simulations (R#1–3) of the receptor in the OTRb and OTRe conformations.

2.1. Mg^{2+} ion coordination

In both conformations, the ion exhibits an octahedral coordination geometry containing four water molecules (W1–4, not resolved in the cryo-EM structure [28]), along with E42 and D100 (Fig. 2B). D100 binds directly to the metal ion, as established by the experimental structure [28]. However, E42 forming direct interactions with the metal ion contrasts with the water-mediated interaction suggested in ref. [28] (see[3]), but it is consistent with both the E42A and D100A mutations decreasing OT binding affinity and losing Mg^{2+}-dependency [28,37]. Moreover, attempts made to add one or two water molecules bridging the Mg^{2+} ion and E42, as suggested by reference [28], followed by system minimization and equilibration steps, consistently resulted in a octahedral coordination geometry of the Mg^{2+} ion with four water molecules and with E42 and D100 as the fifth and sixth ligands. During the simulations, both the Mg^{2+} coordination geometry and the observed Mg^{2+}–ligand distances (Fig. 2C) are stable and in agreement with the values reported in the literature [41–43]. This suggested that the Mg^{2+} parametrization of Jiang et al. [52], used in this work, is adequate to describe the metal ion coordination. In addition, *i*) the E42 backbone NH group keeps an H-bond with the L38 and A39 carbonyl oxygen atoms for 67% and 44% of the simulation time, respectively (Figs. S6 and S7); and *ii*) the D100 backbone N forms an H-bond with the Q96 backbone carbonyl oxygen for almost the entire simulation (97%, Fig. S8), while the D100 and Q96 side chains are involved in an additional H-bond for 62% of the simulated time (Fig. S9).[4] These interactions are present in the experimental structure and are supported by mutagenesis data for Q96 [28], further supporting the reliability of the E42 and D100 interaction network observed in the simulations. Moreover, the other four Mg^{2+} ligands are water molecules, undetected experimentally most likely due to the limited resolution of the cryo-EM density [53].

2.2. Implications for ligand binding

The OT C-terminal portion forms direct or water-mediated hydrogen bonds with three of these Mg^{2+}-coordinated waters for a significant part of the simulations (W1–3 in Fig. 3A and Figs. S12-S15). These obviously did not emerge from the cryo-EM structure. In particular, the interaction observed between Pro^7 and the W2 and W3 waters could provide a rationale for the slight decrease in OT affinity observed for [Thr^4,Gly^7]OT in the presence of Mg^{2+} [44]. Indeed, the replacement of Pro^7 with a very flexible residue, such as a glycine, could increase the conformational space explored by the backbone oxygen of such a residue and partially interfere with the correct placement of the OT C-terminal region without compromising binding of the remaining OT cyclic portion. These water molecules also act as bridges with receptor residues: W1 forms H-bonds with A39 the carbonyl (35%, Fig. S16), while waters W2 and W3 interact with residues Pro^7, Leu^8, Gly^9 of OT, as well as the terminal OT -NH_2 moiety.[5] The proximity of the OT C-terminal amide to the magnesium polyhedron, not observed in the cryo-EM structure [28], could explain why this modification increases OT binding affinity compared to the non-amidated OT [54]. The OT N-terminal part binds inside the receptor orthosteric binding site, both in the Mg(II)-bound receptor and the apo-receptor [37], as observed in the cryo-EM structure. The reduced OTR affinity of [D-Tyr^2]OT relative to native OT both in the presence or in the absence of Mg^{2+} [47] can be explained as follows: Inverting the chirality of Tyr^2 Cα would create steric clashes with OTR residues Q96, K116, and Q119 and break the OT Tyr^2 phenolic Oζ H-bond with the L316 backbone O (see Fig. S1, the H-bond is present for the 37% of the simulation time, Fig. S22) and with the S319 hydroxyl Oγ (26% of the time, Fig. S23). The loss of such interactions impacting OT binding affinity is in line with mutagenesis data for the Ala substitutions of Q96, K116, Q119, L316 and S319 [37].

The presence of an arginine residue (R34), located on the OTR N-term, in the second coordination shell of a magnesium ion, as noticed in the cryo-EM structure [28], is rare. A MetalPDB database [55,56] search performed here shows that this it is found in only two other proteins whose structure has been solved experimentally: the MTH1675 protein from *Methanobacterium thermoautotrophicum* (PDB ID 1T57) and the pyruvate carboxylase from *Rhizobium etli* (PDB ID 2QF7). In our simulations, this structural feature is mostly maintained: the R34 guanidinium group Cζ atom remains between 0.5 and 1.0 nm from the metal ion for more than 60% of the simulation time (Fig. 3B). This is in line with the strong impact of R34 truncation or mutation on OT binding affinity [57] and OT-dependent receptor activation [28]. For the rest of the time, R34 – and consequently the OTR N-terminal portion – moves away from the magnesium coordination sphere and from the OT C-terminal portion, opening one side of the external OT binding pocket. This dynamic R34-OT interaction is compatible with the lack of a clear density for R34 in the Mg^{2+}-free cryo-EM structure of the OTR-OT complex (PDB ID 7QVM) [37]. Thus, the metal ion induces a shift in the conformational preferences of R34, resulting in additional interactions with the ligand,

[3] This difference with respect to the structure could be caused by the fact that water molecules are far less mobile at the temperature of the experiment (the solution containing the protein complex was vitrified into liquid ethane at 184.50 K) than in solution (in our simulations at 303.15 K), and/or by difficulties in interpreting the electron density – the structure has an overall resolution of 0.290 nm, but the local resolution reported for OTR is relatively low (0.330 nm, see extended data in ref. [28]) – and/or by force field artefacts.

[4] In addition, in OTRb R#2, the E42 carboxyl group always forms an H-bond with the OT NH_2 terminus (Figure S10) and the D100 backbone oxygen interacts with the R34 guanidinium group for 6% of the time (Figure S11).

[5] Specifically, W3 H-bonds to the OT amide N atom for 12% of the simulation time, to the backbone oxygen atoms of Leu^8, Gly^9, and Pro^7 for 11%, 7% and 6% of the simulation time, respectively, while W2 H-bonds to the Pro^7 backbone O for 12% of the time (Figures S17-S21).

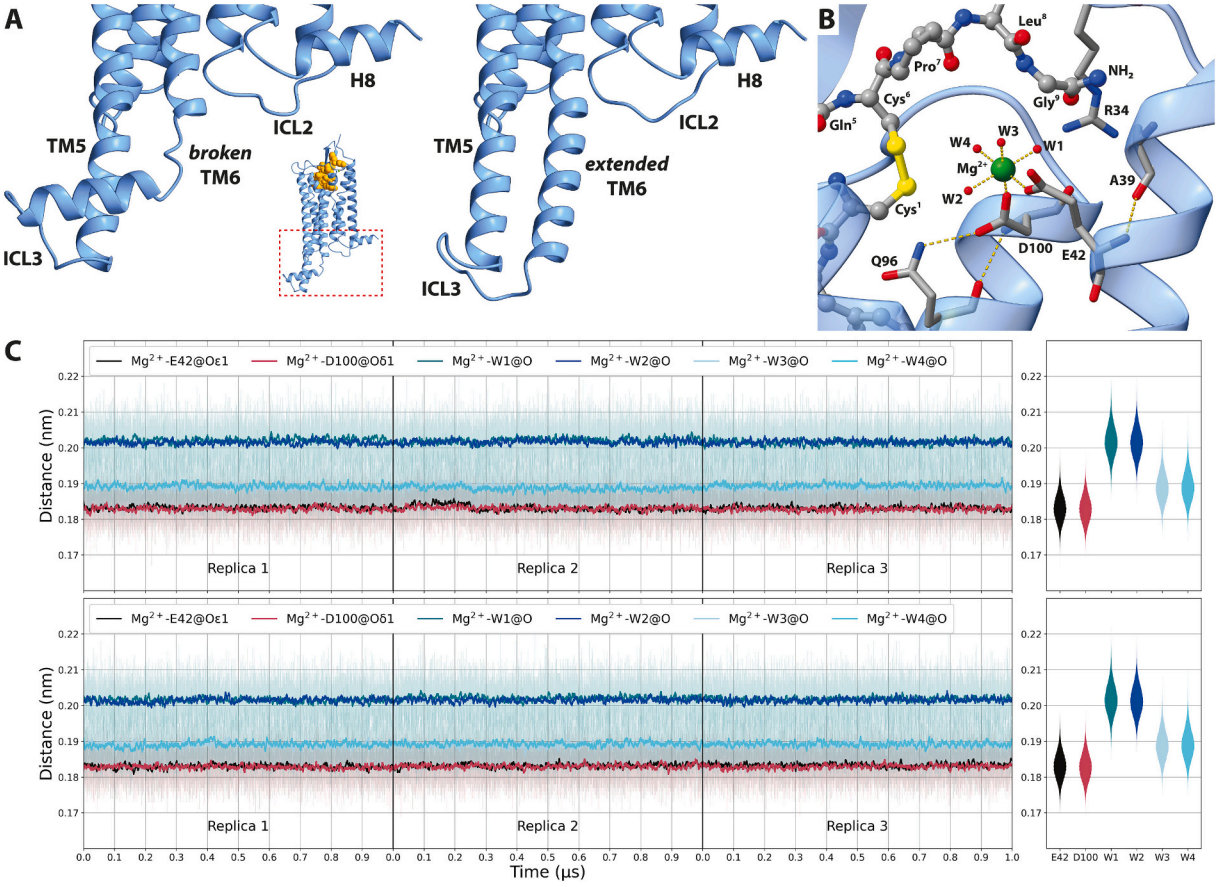

Fig. 2. (**A**) Detail of OTRb (left) and OTRe (right) in the modelled TM5-ICL3-TM6 region. The red dotted box in the inset shows the region displayed in the full-length OTR structure. The OTR ribbons are shown in light blue, while OT is shown in orange spheres. (**B**) Detail of the Mg^{2+} ion coordination sphere in both OTRb and OTRe systems after equilibration. Hydrogen atoms have been hidden to improve figure clarity. OTR is in light blue ribbons and relevant residues are in sticks coloured according to the atom type. OT residues, the Mg^{2+} ion and the water molecules are in ball-and-sticks representation with the atoms coloured according to the atom type. Coordination bonds with the Mg^{2+} ion and relevant H-bonds are reported using yellow dashed lines. (**C**) Distance of the first coordination sphere ligands from the Mg^{2+} ion as a function of the simulation time for OTRb (top) and OTRe (bottom) systems. Mg^{2+}-E42(Oε1) and Mg^{2+}-D100(Oδ1) distances are in black and red, respectively, while the distance between the Mg^{2+} and W1, W2, W3, and W4 oxygen atoms are in aquamarine blue, blue, light blue and cyan, respectively. The right panels report the distribution of the distance values. The bold lines were obtained by applying a Savitzky–Golay filter [61] in order to cut out the noise. (For interpretation of the references to colour in this figure legend, the reader is referred to the web version of this article.)

which might contribute to the experimentally observed increase in OT affinity in the presence of Mg^{2+}. Another important difference between the cryo-EM structures with and without Mg^{2+} is the cation-π interaction (or lack thereof) of R34 and with F103, located in ECL1 and whose mutation to Ala impacts OT binding affinity [57] and receptor activation [28]. Analysis of the distance between R34 guanidinium Cζ and F103 benzyl Cγ as a function of simulation time shows that these two residues remain within 1.0 nm of one another for about half of the simulation time (Fig. S24), suggesting a role for F103 in the stabilization of the R34 side chain correct orientation with respect to the Mg^{2+} polyhedron.

2.3. Implication for receptor activation

The MD simulations of OTRe R#1–3 and OTRb R#2 keep the receptor in the active state, as shown by the analysis of the A^{100} activation index [58] (Fig. S25). The latter result is interesting considering that the OTRb TM5-ICL3-TM6 region was modelled using the inactive GPCRs as templates in the AlphaFold-Multistate [48,59], whereas the OTRe conformation was modelled using active templates. In contrast, the OTRb replica with a larger shift toward an inactive form in the A^{100} activation index is R#3, which also shows the largest reorganization of the TM5-ICL3-TM6 region bringing the ICL3 loop below the receptor, in a region occupied by the G_q protein in the cryo-EM structure (Fig. S26).

By analysing the OTRb R#1 and R#3 trajectories, in which the protein assumes an inactive conformation, it is possible to notice the movement of the OT C-terminal residues (such as Pro^7) along with second shell magnesium ligands (such as R34) away from the metal ion (Fig. 4 and Fig. S25). These simulations thus highlight a link between inactivation and the release of the OT C-terminal/OTR R34 from the metal ion (Fig. 4 and Fig. S27). This is also consistent with the effect of Mg^{2+} not only on OT binding affinity [44] but also on receptor activation [28]. In addition to the metal ion, we observe that the active/inactive transition of the TM5-ICL3-TM6 region is associated with a TM6 conformational change (Fig. S28). Thus, the TM5-ICL3-TM6 region could act as a lever capable of contributing to inactivation, confirming the importance of this region to receptor/G-protein coupling by acting like an autoregulator of receptor activity [38,39]. The distancing of R34 and/or the OT C-terminal portion from the Mg^{2+} ion is also observed in some replicas of the OTRe system (Fig. 4 and Fig. S27), but without any inactivation process occurring on the microsecond time scale of the simulations, most likely due to the initial extended conformation of the TM5-ICL3-TM6 region. Taken together, these observations suggest that the opening of the N-terminal side of the OT binding cavity achieved through the movement of R34 and the N-terminal region and/or the displacement of the OT C-terminal portion far away from the Mg^{2+} ion is not sufficient to induce OTR inactivation, but contribute to it, together with changes in the TM5-ICL3-TM6 region. In the absence of the magnesium ion, we would expect the following: *i*) the OTR N-terminal and

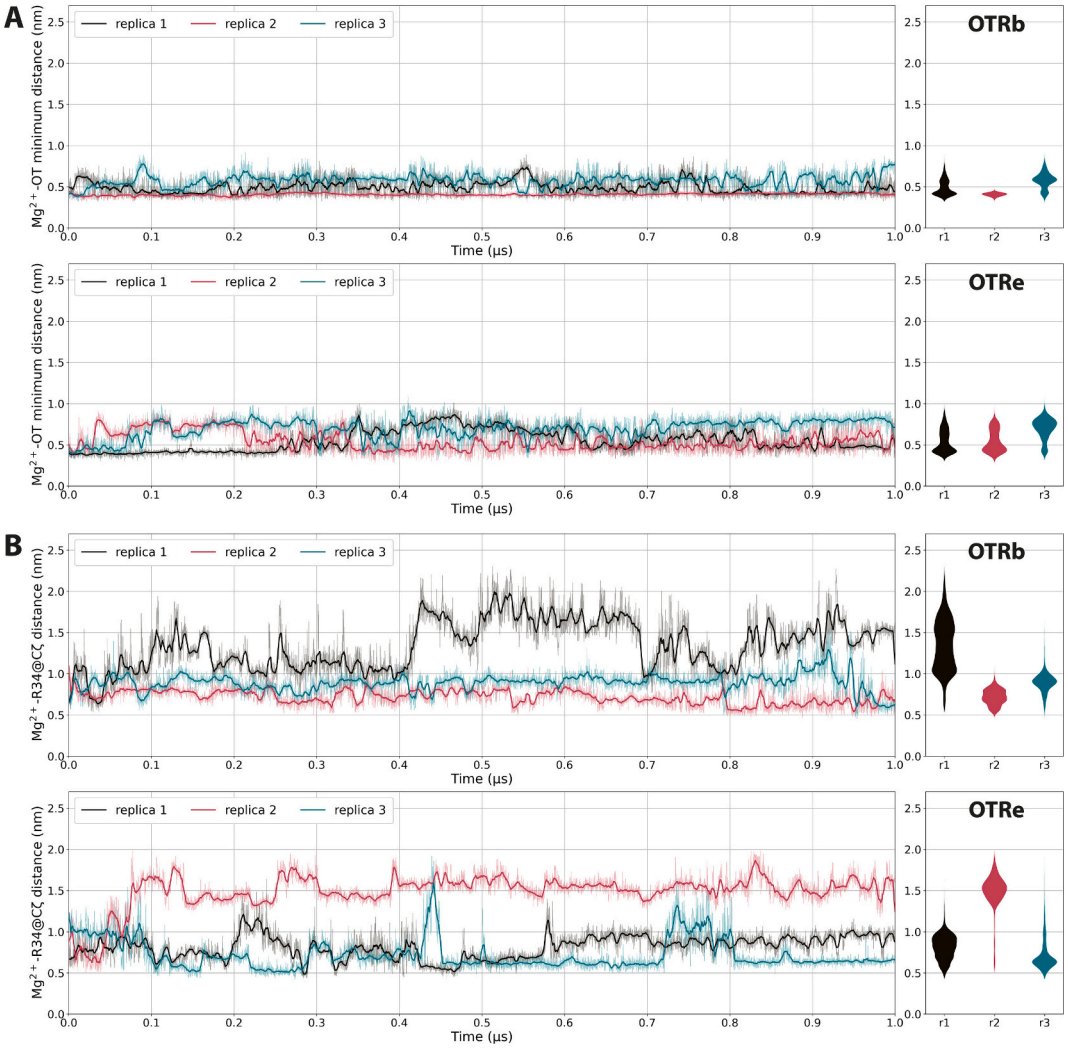

Fig. 3. Minimum distance between the Mg^{2+} ion and OT C-terminal residues (namely Pro^{7}, Leu^{8}, Gly^{9} and the -NH_2 terminal) (**A**) and Mg^{2+}-R34(Cζ) distance (**B**) as a function of the simulation time for OTRb (top panel) and OTRe (bottom panel) systems. Values for the three replicas simulated for each system are in black, dark red and cyan, respectively. Right panels report the distribution of the distance values in the three replicas of each system. The bold lines were obtained by applying a Savitzky-Golay filter [61] in order to cut out the noise. (For interpretation of the references to colour in this figure legend, the reader is referred to the web version of this article.)

the OT C-terminal regions would become more flexible and, as a consequence, one side of the OT binding site would become floppier and the OT C-terminal region/receptor interactions would weaken; and *ii*) the interface between TM1 and TM2 (where E42 and D100 are located) would become more mobile. These hypothesis might be corroborated by a comparison of the cryo-EM structures of OTR bound to OT in the presence (PDB ID 7RYC) and in the absence of any Mg^{2+} ion (PDB ID 7QVM): in the latter four fewer residues were resolved in the N-terminal region with respect to the structure used in the present simulations (therefore, R34 is absent in the structure where magnesium is not present) and the ECL2 β-hairpin is partially unsolved. In addition, the OT C-terminal region is in a slightly different conformation, even though the N-terminal part bound to the OTR orthosteric site is nearly superimposable. Thus, the poorer resolution and the partial inability to resolve some residues in the outer region of the OTR binding site in the absence of magnesium might indeed be consistent with our assumptions.

3. Conclusions

The Mg^{2+} coordination polyhedron, fully characterized here for the first time, plays a crucial role both for OT binding and OTR activation. The simulations performed on the OTR-OT complex with bound Mg^{2+} in two starting conformations of the TM5-ICL3-TM6 region suggest that receptor inactivation may occur if the OT C-terminal residues and R34 – which regulates the conformation of OTR N-terminal – move away from the Mg^{2+} ion. However, the conformation assumed by the TM5-ICL3-TM6 region is also crucial for the active/inactive transition. The characterization of the Mg^{2+} coordination sphere in the OTR-OT complex also has implications for the closely related vasopressin receptors (V1aR, V1bR and V2R in humans). The two acidic residues directly coordinating the Mg^{2+} ion ($E^{1.35}$ and $D^{2.65}$) are conserved in V1aR and V1bR, whose activation is also dependent on Mg^{2+}, while the aspartate is replaced by a lysine in the Mg^{2+}-insensitive V2R. In the absence of experimental structures of V1aR and V1bR with Mg^{2+} bound, the combination of AlphaFold-Multistate and molecular dynamics simulations, as used here, could provide reliable structural models of such complexes. In conclusion, given the limitations of cryo-EM in resolving water molecules and metal ions [53], complementary molecular dynamics emerge as an excellent strategy to fully characterize metal coordination and thus understand its impact on receptor structure and function. An accurate description of the metal ion, either using state-of-the-art force fields [52] or even quantum mechanics/molecular mechanics approaches [60], is

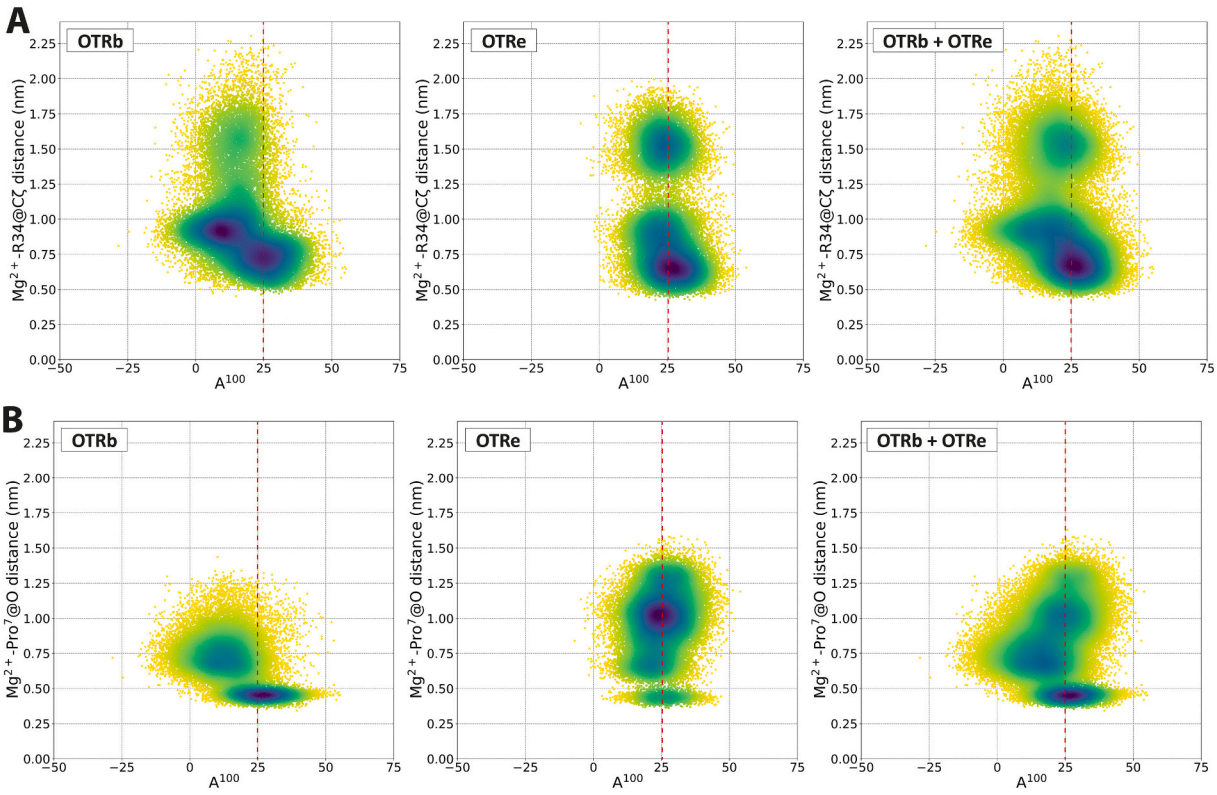

Fig. 4. Distance between the Mg^{2+} ion and R34(Cζ) (**A**) or Pro^{7}(O) (**B**) reported as a function of the A^{100} activation index for each frame of the OTRb and OTRe simulations (left and central panels) and by summing up the simulations on both system (right panels). The dot's colour changes from yellow to dark blue as their density increases. The vertical red dashed line highlights the A^{100} activation index boundary between states ($A^{100} \geq +25$ = active) [58]. (For interpretation of the references to colour in this figure legend, the reader is referred to the web version of this article.)

essential to ensure the reliability of such MD simulations.

Acknowlegdments

F.M. was supported by the Italian Ministry of Education, University and Research (RFO grant 2024) and by Consorzio Interuniversitario Risonanze Magnetiche di Metallo Proteine (CIRMMP). S.A.S. was supported by a Study Grants for the Preparation of the Thesis Abroad awarded by the Department of Pharmacy and Biotechnology of the University of Bologna. The authors gratefully acknowledge the computing time provided to them at the NHR Center NHR4CES at RWTH Aachen University (project number p0020569). This center is funded by the Federal Ministry of Research, Technology and Space, and the state governments participating on the basis of the resolutions of the GWK for national high-performance computing at universities (www.nhr-verein.de/unsere-partner).

CRediT authorship contribution statement

Francesco Musiani: Writing – review & editing, Writing – original draft, Visualization, Validation, Supervision, Software, Resources, Project administration, Methodology, Investigation, Funding acquisition, Formal analysis, Data curation, Conceptualization. **Samira Al Sadi:** Investigation, Data curation. **Alejandro Giorgetti:** Writing – original draft, Supervision, Investigation, Conceptualization. **Mercedes Alfonso-Prieto:** Writing – review & editing, Writing – original draft, Supervision, Resources, Project administration, Methodology, Funding acquisition, Conceptualization. **Paolo Carloni:** Writing – review & editing, Writing – original draft, Supervision, Resources, Project administration, Methodology, Funding acquisition, Conceptualization.

Declaration of competing interest

The authors declare that they have no known competing financial interests or personal relationships that could have appeared to influence the work reported in this paper.

Appendix A. Supplementary data

Supplementary data to this article can be found online at https://doi.org/10.1016/j.jinorgbio.2026.113309.

Data availability

All MD simulations conducted in this study have been uploaded to MDposit (https://mdposit.mddbr.eu), an open-access platform designed to provide web-based access to atomistic MD simulations. Accession: MD-A00400 and MD-A00401 for the OTRb and OTRe systems, respectively.

References

[1] R. Fredriksson, M.C. Lagerstrom, L.G. Lundin, H.B. Schioth, Mol. Pharmacol. 63 (2003) 1256–1272.
[2] J.S. Lorente, A.V. Sokolov, G. Ferguson, H.B. Schioth, A.S. Hauser, D.E. Gloriam, Nat. Rev. Drug Discov. 24 (2025) 458–479.
[3] B. Zarzycka, S.A. Zaidi, B.L. Roth, V. Katritch, Pharmacol. Rev. 71 (2019) 571–595. Elsevier.
[4] R. Zou, X. Wang, S. Li, H.C.S. Chan, H. Vogel, S. Yuan, WIREs Comput. Mol. Sci. 12 (2022) e1565. John Wiley & Sons, Ltd.
[5] L. Pirona, F. Ballabio, M. Alfonso-Prieto, R. Capelli, J. Chem. Inf. Model. 64 (2024) 2971–2978.
[6] J. Yu, L.E. Gimenez, C.C. Hernandez, Y. Wu, A.H. Wein, G.W. Han, K. McClary, S. R. Mittal, K. Burdsall, B. Stauch, L. Wu, S.N. Stevens, A. Peisley, S.Y. Williams, V. Chen, G.L. Millhauser, S. Zhao, R.D. Cone, R.C. Stevens, Science 368 (2020) 428–433.

[7] N.A. Heyder, G. Kleinau, D. Speck, A. Schmidt, S. Paisdzior, M. Szczepek, B. Bauer, A. Koch, M. Gallandi, D. Kwiatkowski, J. Burger, T. Mielke, A.G. Beck-Sickinger, P. W. Hildebrand, C.M.T. Spahn, D. Hilger, M. Schacherl, H. Biebermann, T. Hilal, P. Kuhnen, B.K. Kobilka, P. Scheerer, Cell Res. 31 (2021) 1176–1189.
[8] H. Israeli, O. Degtjarik, F. Fierro, V. Chunilal, A.K. Gill, N.J. Roth, J. Botta, V. Prabahar, Y. Peleg, L.F. Chan, D. Ben-Zvi, P.J. McCormick, M.Y. Niv, M. Shalev-Benami, Science 372 (2021) 808–814.
[9] S. Ma, Y. Chen, A. Dai, W. Yin, J. Guo, D. Yang, F. Zhou, Y. Jiang, M.W. Wang, H. E. Xu, Cell Res. 31 (2021) 1061–1071.
[10] H. Zhang, L.N. Chen, D. Yang, C. Mao, Q. Shen, W. Feng, D.D. Shen, A. Dai, S. Xie, Y. Zhou, J. Qin, J.P. Sun, D.H. Scharf, T. Hou, T. Zhou, M.W. Wang, Y. Zhang, Cell Res. 31 (2021) 1163–1175.
[11] W. Feng, Q. Zhou, X. Chen, A. Dai, X. Cai, X. Liu, F. Zhao, Y. Chen, C. Ye, Y. Xu, Z. Cong, H. Li, S. Lin, D. Yang, M.W. Wang, Cell Discov. 9 (2023) 81.
[12] P. Luo, W. Feng, S. Ma, A. Dai, K. Wu, X. Chen, Q. Yuan, X. Cai, D. Yang, M. W. Wang, H. Eric Xu, Y. Jiang, Cell Res. 33 (2023) 46–54.
[13] X. Hu, D. Provasi, S. Ramsey, M. Filizola, Biophys. J. 118 (2020) 909–921.
[14] H.C.S. Chan, Y. Xu, L. Tan, H. Vogel, J. Cheng, D. Wu, S. Yuan, ACS Cent. Sci. 6 (2020) 274–282.
[15] R.K. Rude, in: A.C. Ross, B. Caballero, R.J. Cousins, K.L. Tucker, T.R. Ziegler (Eds.), Modern Nutrition in Health and Disease, Lippincott Williams & Wilkins, Baltimore, U.S.A., 2012, pp. 159–175.
[16] D. Fiorentini, C. Cappadone, G. Farruggia, C. Prata, Nutrients 13 (2021).
[17] K. Jomova, M. Makova, S.Y. Alomar, S.H. Alwasel, E. Nepovimova, K. Kuca, C. J. Rhodes, M. Valko, Chem. Biol. Interact. 367 (2022) 110173.
[18] T. Liu, L. Wang, S. Pei, S. Yang, J. Wu, W. Liu, Q. Wu, Analyst 150 (2025) 2979–2999.
[19] A. Botturi, V. Ciappolino, G. Delvecchio, A. Boscutti, B. Viscardi, P. Brambilla, Nutrients 12 (2020).
[20] G.N. Ekinci, N. Sanlier, Exp. Gerontol. 172 (2023) 112072.
[21] A. Kumar, S. Mehan, A. Tiwari, Z. Khan, G.D. Gupta, A.S. Narula, R. Samant, Curr. Pharm. Des. 30 (2024) 3074–3107.
[22] F. Chen, J. Wang, Y. Cheng, R. Li, Y. Wang, Y. Chen, T. Scott, K.L. Tucker, Adv. Nutr. 15 (2024) 100272.
[23] B. Jurek, I.D. Neumann, Physiol. Rev. 98 (2018) 1805–1908. American Physiological Society.
[24] K.L. Bales, Compr. Psychoneuroendocrinol. 16 (2023) 100203.
[25] C.S. Carter, Compr. Psychoneuroendocrinol. 15 (2023) 100189.
[26] X. Han, Y. Ma, Neuroscientist 31 (2024) 409–424.
[27] G. Gimpl, F. Fahrenholz, Physiol. Rev. 81 (2001) 629–683.
[28] J.G. Meyerowitz, M.J. Robertson, X. Barros-Alvarez, O. Panova, R.M. Nwokonko, Y. Gao, G. Skiniotis, Nat. Struct. Mol. Biol. 29 (2022) 274–281.
[29] M. Busnelli, B. Chini, Curr. Top. Behav. Neurosci. 35 (2018) 3–29.
[30] D. Gulliver, E. Werry, T.A. Reekie, T.A. Katte, W. Jorgensen, M. Kassiou, Trends Pharmacol. Sci. 40 (2019) 22–37.
[31] R.P. Chaulagain, Y. Shrestha, H. Shrestha, R. Bhandari, P. Gurung, Ann. Med. Surg. (Lond.) 87 (2025) 1479–1486.
[32] M. Meyer, B. Jurek, M. Alfonso-Prieto, R. Ribeiro, V.M. Milenkovic, J. Winter, P. Hoffmann, C.H. Wetzel, A. Giorgetti, P. Carloni, I.D. Neumann, Mol. Psychiatry 27 (2022) 907–917.
[33] M. Malik, M.D. Ward, Y. Fang, J.R. Porter, M.I. Zimmerman, T. Koelblen, M. Roh, A.I. Frolova, T.P. Burris, G.R. Bowman, P.I. Imoukhuede, S.K. England, ACS Pharmacol. Transl. Sci. 4 (2021) 1543–1555.
[34] M.S. Soloff, Life Sci. 25 (1979) 1453–1460.
[35] A.F. Pearlmutter, M.S. Soloff, J. Biol. Chem. 254 (1979) 3899–3906.
[36] V.N. Bharadwaj, J. Meyerowitz, B. Zou, M. Klukinov, N. Yan, K. Sharma, D.J. Clark, X. Xie, D.C. Yeomans, Pharmaceutics 14 (2022).
[37] Y. Waltenspuhl, J. Ehrenmann, S. Vacca, C. Thom, O. Medalia, A. Pluckthun, Nat. Commun. 13 (2022) 4153.
[38] F. Sadler, N. Ma, M. Ritt, Y. Sharma, N. Vaidehi, S. Sivaramakrishnan, Nature 615 (2023) 734–741.
[39] J. Wess, Trends Pharmacol. Sci. 44 (2023) 492–494.
[40] Y. Waltenspuhl, J. Schoppe, J. Ehrenmann, L. Kummer, A. Pluckthun, Sci. Adv. 6 (2020) eabb5419.
[41] M. Bazayeva, C. Andreini, A. Rosato, Acta Crystallogr. D Struct. Biol. 80 (2024) 362–376.
[42] G.Y. Lin, Y.C. Su, Y.L. Huang, K.Y. Hsin, Nucleic Acids Res. 52 (2024) D483–D493.
[43] H. Zheng, D.R. Cooper, P.J. Porebski, I.G. Shabalin, K.B. Handing, W. Minor, Acta Crystallogr. D Struct. Biol. 73 (2017) 223–233.
[44] F.A. Antoni, S.E. Chadio, Biochem. J. 257 (1989) 611–614.
[45] J. Lowbridge, M. Manning, J. Haldar, W.H. Sawyer, J. Med. Chem. 20 (1977) 120–123.
[46] G.L. Stahl, R. Walter, J. Med. Chem. 20 (1977) 492–495.
[47] V.J. Hruby, D.A. Upson, D.M. Yamamoto, C.W. Smith, R. Walter, J. Am. Chem. Soc. 101 (1979) 2717–2721. American Chemical Society.
[48] L. Heo, M. Feig, Proteins 90 (2022) 1873–1885.
[49] I.D. Pogozheva, G.A. Armstrong, L. Kong, T.J. Hartnagel, C.A. Carpino, S.E. Gee, D. M. Picarello, A.S. Rubin, J. Lee, S. Park, A.L. Lomize, W. Im, J. Chem. Inf. Model. 62 (2022) 1036–1051.
[50] B. Marlow, A. Vogel, G. Kuenze, M. Pankonin, F. Reinhardt, P.F. Stadler, P. W. Hildebrand, J. Meiler, Biophys. J. 124 (2025) 1930–1943.
[51] G. Gimpl, K. Burger, E. Politowska, J. Ciarkowski, F. Fahrenholz, Exp. Physiol. 85 (2000) 41S–49S. Spec No.
[52] Y. Jiang, H. Zhang, W. Feng, T. Tan, J. Chem. Inf. Model. 55 (2015) 2575–2586.
[53] G. Pintilie, W. Chiu, Acta Crystallogr. D Struct. Biol. 77 (2021) 1142–1152.
[54] B.M. Ferrier, V. Du Vigneaud, J. Med. Chem. 9 (1966) 55–57.
[55] C. Andreini, G. Cavallaro, S. Lorenzini, A. Rosato, Nucleic Acids Res. 41 (2013) D312–D319.
[56] V. Putignano, A. Rosato, L. Banci, C. Andreini, Nucleic Acids Res. 46 (2018) D459–D464.
[57] V.J. Wesley, S.R. Hawtin, H.C. Howard, M. Wheatley, Biochemistry 41 (2002) 5086–5092. American Chemical Society.
[58] P. Ibrahim, D. Wifling, T. Clark, J. Chem. Inf. Model. 59 (2019) 3938–3945.
[59] G. Pandy-Szekeres, J. Caroli, A. Mamyrbekov, A.A. Kermani, G.M. Keseru, A. J. Kooistra, D.E. Gloriam, Nucleic Acids Res. 51 (2023) D395–D402.
[60] F.K. Schackert, J. Biedermann, S. Abdolvand, S. Minniberger, C. Song, A.J. R. Plested, P. Carloni, H. Sun, J. Chem. Inf. Model. 63 (2023) 1293–1300.
[61] A. Savitzky, M.J.E. Golay, Anal. Chem. 36 (1964) 1627–1639. American Chemical Society.